Wave reflection at the origin of a first-generation branch artery and target organ protection: the AGES-Reykjavik study

Haidar, M.A.; Buchem, M.A. van; Sigurdsson, S.; Gotal, J.D.; Gudnason, V.; Launer, L.J.; Mitchell, G.F.

Hypertension

ARTERIAL STIFFNESS

Wave Reflection at the Origin of a First-Generation Branch Artery and Target Organ Protection

The AGES-Reykjavik Study

Michael A. Haidar, Mark A. van Buchem, Sigurdur Sigurdsson, John D. Gotal, Vilmundur Gudnason, Lenore J. Launer, Gary F. Mitchell

ABSTRACT: Excessive pressure and flow pulsatility in first-generation branch arteries are associated with microvascular damage in high-flow organs like brain and kidneys. However, the contribution of local wave reflection and rereflection to microvascular damage remains controversial. Aortic flow, carotid pressure, flow and hydraulic power, brain magnetic resonance images, and cognitive scores were assessed in AGES-Reykjavik study participants without history of stroke, transient ischemic attack, or dementia (N=668, 378 women, 69–93 years of age). The aorta-carotid interface was generalized as a markedly asymmetrical bifurcation, with a large parent vessel (proximal aorta) branching into small (carotid) and large (distal aorta) daughter vessels. Local reflection coefficients were computed from aortic and carotid characteristic impedances. The bifurcation reflection coefficient, which determines pressure amplification in both daughter vessels, was low (0.06±0.03). The carotid flow transmission coefficient was low (0.11±0.04) and associated with markedly lower carotid versus aortic flow pulsatility (waveform SD, 7.2±2.0 versus 98.7±21.8 mL/s, $P<0.001$), pulsatility index (1.8±0.5 versus 4.5±0.6, $P<0.001$), and pulsatile power percentage (10±4% versus 25±5%, $P<0.001$). Transmitted as compared to incident pulsatile power (19.0±9.8 versus 35.9±17.8 mW, $P<0.001$) was further reduced by reflection (−4.3±2.7 mW) and rereflection (−12.5±8.1 mW) within the carotid. Higher carotid flow pulsatility correlated with lower white matter volume (R=−0.130, $P<0.001$) and lower memory scores (R=−0.161, $P<0.001$). Marked asymmetry of characteristic impedances at aorta-branch artery bifurcations limits amplification of pressure, markedly reduces absolute and relative pulsatility of transmitted flow and hydraulic power into first-generation branch arteries, and thereby protects the downstream local microcirculation from pulsatile damage. (*Hypertension*. 2021;77:1169-1177. DOI: 10.1161/HYPERTENSIONAHA.120.16696.) ● **Data Supplement**

Key Words: aorta ■ dementia ■ magnetic resonance image ■ microcirculation ■ stroke

Age-related dementias affect ≈5.8 million people in the United States.[1] By 2050, the prevalence is projected to increase to over 13.8 million.[1] Cardiovascular risk factors, including arterial stiffness, are risk factors for dementias of all types and represent important potentially modifiable targets for intervention.[2] Pressure and flow pulsatility in the macrocirculation and microcirculation are associated with microvascular damage in target organs like the brain and kidneys.[3–7] Wave reflection at the origin of a first-generation branch artery (FGBA) arising from the aorta represents a possible mechanism that could limit the pulsatility of flow and power transmitted into these arteries.[8] However, some have speculated that since the aorta-carotid bifurcation is relatively well matched, with a reflection coefficient of 0% to 15%, any effect of local wave reflection on transmitted power at the junction is trivial, with 97% and 100% of incident power transmitted.[9,10] Furthermore, larger bifurcation reflection coefficients increase transmitted pulsatile pressure, which should be deleterious

Hypertension is available at www.ahajournals.org/journal/hyp

Novelty and Significance

What Is New?

- The present analysis provides the first detailed description of pulsatile pressure, flow, and power dynamics at a generalized asymmetrical bifurcation in the aorta.

What Is Relevant?

- Excessive pulsatile power is harmful in the microcirculation of high-flow organs like the brain and kidneys and is exacerbated by aortic stiffening. Cardiovascular disease risk factors associated with aortic stiffening

represent important potentially modifiable targets for intervention.

Summary

The general structure of markedly asymmetrical bifurcations at stiff first-generation branch arteries arising from a compliant aorta optimally limits pulsatile power transmission into the branch vasculature and protects the fragile microcirculation.

Nonstandard Abbreviations and Acronyms

FGBA	first-generation branch artery

in terms of downstream organ function.[11] Others have observed that bifurcations in the arterial system are generally impedance-matched in the forward, but not the backward direction, optimally transmitting forward hydraulic power while causing backward-traveling power to be trapped in daughter arteries by rereflection.[12–15] We examined relations of the aorta-carotid bifurcation reflection coefficient and carotid flow transmission coefficient with the pulsatile flow and hydraulic power in the common carotid arteries. We hypothesize that the highly asymmetrical structure of bifurcations, consisting of the low characteristic impedance aorta giving rise to a high characteristic impedance FGBA and continuation of the low characteristic impedance aorta, limits amplification of transmitted pressure while markedly limiting pulsatility of flow and power transmitted into the FGBA. We further hypothesize that the limitation of pulsatile power entering the FGBA circulation is attributable to low initial transmission as well as rereflection at the origin of the FGBA, both of which are dependent on a high FGBA reflection coefficient.

METHODS

Data Availability

The data that support the findings of this study are available from the corresponding author upon reasonable request.

Study Participants

The rationale and design of the AGES-Reykjavik study have been presented.[16] Between 2002 and 2006, a total of 5764 men and women participated in detailed evaluations of cardiovascular, neurocognitive, musculoskeletal, and metabolic phenotypes. AGES-Reykjavik was approved by the National

Bioethics Committee in Iceland, which acts as the institutional review board for the Icelandic Heart Association (approval number VSN-00-063), and by the National Institute on Aging Intramural Review Board. All participants gave written informed consent.

Data Acquisition and Analysis

The hemodynamic data acquisition, brain magnetic resonance imaging, and cognitive function testing protocols have been described.[8,16–22] Please see http://hyper.ahajournals.org for the Data Supplement with additional details. Briefly, signal averaged tonometry waveforms were calibrated using mean and diastolic pressure from the brachial waveform, which was calibrated to systolic and diastolic brachial cuff pressure.[23] Aortic and common carotid artery flows were analyzed from digitized Doppler audio data using a semiautomated signal-averaging approach as detailed previously.[24] Flow velocity waveforms from each common carotid artery were multiplied by the respective artery cross-sectional area to obtain volumetric flow rates. Right and left volumetric carotid flow waveforms were then summed to create one aggregate carotid flow waveform. Peripheral vascular resistance was computed as mean arterial pressure divided by mean flow. Aortic and carotid characteristic impedances were calculated by dividing the peak derivative of pressure by the peak derivative of flow.[25] Normalized impedance was calculated by dividing characteristic impedance by the associated peripheral resistance. Flow pulsatility index was computed for carotid and aortic waveforms by dividing the flow pulse amplitude (peak flow minus flow at the onset of the systolic upstroke) by mean flow. Global flow pulsatility was

assessed as the flow SD, $QSD = \sqrt{\dfrac{\sum_{t=0}^{T}\left(Q_t - \bar{Q}\right)^2}{T}}$, where $\bar{Q}$

represents mean flow.[26]

Total hydraulic power (in Watts, W) was calculated as the average of the point-by-point product of time-resolved pressure (P) and flow (Q) waveforms: $\Pi = \dfrac{1}{T}\sum_{t=0}^{T}\left(P_t \times Q_t\right)$, where t represents time, and T represents the period of one cardiac cycle.[27] For simplicity, the above formula will henceforth be denoted as: $\Pi = P \times Q$. Mean power (units of W) was calculated as mean arterial pressure multiplied by mean flow. Pulsatile power was calculated as the difference between total power and mean power.

Wave Separation Analysis

Transit time from proximal aorta to the flow measurement site in the common carotid artery, ≈1 cm proximal to the carotid sinus, was assessed as foot-foot delay between aortic and carotid flow waveforms. This total delay was divided into 2 equal segment delays, assuming that the transit times from aortic root to common carotid origin and from common carotid origin to the flow measurement site in the distal common carotid were comparable. Distal common carotid forward and backward pressure and flow waveforms were obtained by time-domain wave separation analysis.[28] Distal reflection factor was computed by dividing backward wave amplitude by forward wave amplitude. To estimate the pressure and flow waves at the common carotid origin, we shifted forward pressure and flow waves one segment delay earlier and backward pressure and flow wave one segment delay later, then recombined the forward and backward waveforms (Figure S1 in the Data Supplement).

Bifurcation Model

The aorta-carotid interface was modeled as a simple bifurcation, where the proximal aorta (vessel 1) branches into 2 daughter vessels (Figure 1). The lumped right and left common carotid arteries represent one branch (vessel 2), and the downstream aorta and distal vasculature represent the other branch (vessel 3). The 3 vessels have characteristic admittances (reciprocal of characteristic impedance) of A_1, A_2 and A_3, respectively. To estimate distal aortic characteristic impedance, we assumed constant local pulse wave velocity and mean flow velocity in the aorta proximal and distal to the origin of the common carotid arteries.[8] Under these conditions, the distal impedance can be assumed to be equal to the proximal impedance scaled in proportion to the drop in mean volume flow:

$$Z_{distal} = Z_{proximal} \times \left(\frac{\bar{Q}_{proximal}}{\bar{Q}_{distal}} \right),$$ where Z denotes characteristic

impedance and $\bar{Q}$ denotes mean flow. The bifurcation reflection coefficient is as follows: $\Gamma_1 = \dfrac{A_1 - A_2 - A_3}{A_1 + A_2 + A_3}$. The reflection coefficients for retrograde waves exiting branches 2 and 3 are

$$\Gamma_{2rr} = \frac{-A_1 + A_2 - A_3}{A_1 + A_2 + A_3} \text{ and } \Gamma_{3rr} = \frac{-A_1 - A_2 + A_3}{A_1 + A_2 + A_3}, \text{ respectively.}$$

For mathematical convenience, we define the quantities $\Gamma_2 = -\Gamma_{2rr}$ and $\Gamma_3 = -\Gamma_{3rr}$, to express the values with respect to antegrade waves entering a single branch, where the reflection coefficient has the same magnitude but opposite sign as for retrograde waves. The transmission coefficient for pressure is $(1+\Gamma_1)$, while the transmission coefficients for flow in daughter branches 2 and 3 are $\dfrac{2A_2}{A_1 + A_2 + A_3}$, equivalent to $(1-\Gamma_2)$, and $\dfrac{2A_3}{A_1 + A_2 + A_3}$, equivalent to $(1-\Gamma_3)$, respectively, resulting in power transmission coefficients in the 2 daughter vessels of $(1+\Gamma_1) \times (1-\Gamma_2)$ and $(1+\Gamma_1) \times (1-\Gamma_3)$, respectively. Please see http://hyper.ahajournals.org for the Data Supplement with further details.

Using the previously defined notation for average hydraulic power over the cardiac period, forward wave hydraulic power in the aortic root is defined as follows: $\Pi f_{Ao} = Pf_{Ao} \times Qf_{Ao}$, where Pf_{Ao} and Qf_{Ao} are the initial forward-traveling pressure and flow waveforms (with mean offsets removed) in the proximal aorta.
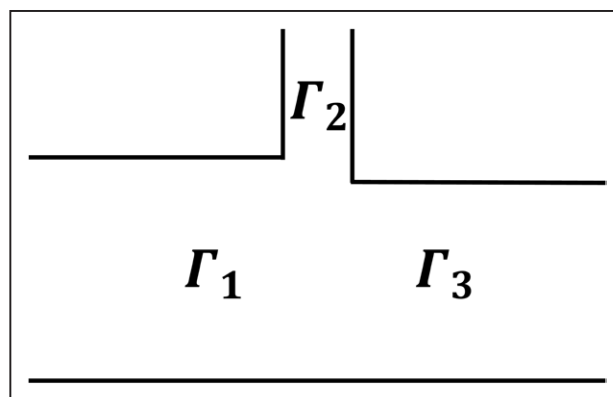

Figure 1. Simplified schematic of the aorta-carotid interface.
We model the aorta-carotid interface as a simple asymmetrical bifurcation in which the proximal aortic segment (branch 1) splits into a carotid branch (branch 2) and the distal aortic segment (branch 3). Γ_1 indicates bifurcation reflection coefficient; Γ_2, carotid reflection coefficient; and Γ_3, distal aortic reflection coefficient.

Forward waves in the carotid were decomposed as the sum of incident and rereflected components: $Pf_{Car} = Pinc_{Car} + Prr_{Car}$ and $Qf_{Car} = Qinc_{Car} + Qrr_{Car}$, where rereflected pressure and flow were computed as follows: $Prr_{Car} = (-\Gamma_2)Pb_{Car}$ and $Qrr_{Car} = (\Gamma_2)Qb_{Car}$ (Figure 2), noting that only a single iteration of reflection and rereflection was considered. Incident pressure was then computed as follows: $Pinc_{Car} = Pf_{Car} - Prr_{Car}$ and incident flow as follows: $Qinc_{Car} = Qf_{Car} - Qrr_{Car}$. Net forward-traveling power was computed as follows: $\Pi f_{Car} = Pf_{Car} \times Qf_{Car} = (Pinc_{Car} + Prr_{Car}) \times (Qinc_{Car} + Qrr_{Car})$. Expanding this product resulted in 4 power components: $Pinc_{Car} \times Qinc_{Car}$ and $Prr_{Car} \times Qrr_{Car}$ represent in-phase incident and rereflected power, respectively, while $Pinc_{Car} \times Qrr_{Car}$ and $Prr_{Car} \times Qinc_{Car}$ represent interaction terms of incident and rereflected waves. Reflected wave hydraulic power was calculated as follows: $\Pi b_{Car} = Pb_{Car} \times Qb_{Car}$.

Statistical Analysis

Sample characteristics, hemodynamic variables, measures of brain structure and function, and components of total pulsatile power in the common carotid arteries were tabulated. Stepwise multivariable linear regression analysis was used to assess relations of local wave reflection with carotid flow pulsatility (assessed as waveform SD) and pulsatile power in the common carotid arteries. Multivariable adjusted partial correlation was performed to examine relations of carotid flow SD and pulsatile power with measures of brain structure and function. Partial correlations were adjusted for previously reported correlates of arterial function and brain structure and function, including age, height, weight, high-density lipoprotein cholesterol level, blood glucose level, use of statin drugs, heart rate, mean arterial pressure, current smoking, presence of depressive symptoms, and education level. Carotid flow SD, pulsatile power, and pulse pressure were skewed and were, therefore, natural logarithm transformed. For all models, continuous dependent and independent variables were first converted to sex-specific Z scores. A 2-sided $P<0.05$ was considered significant.
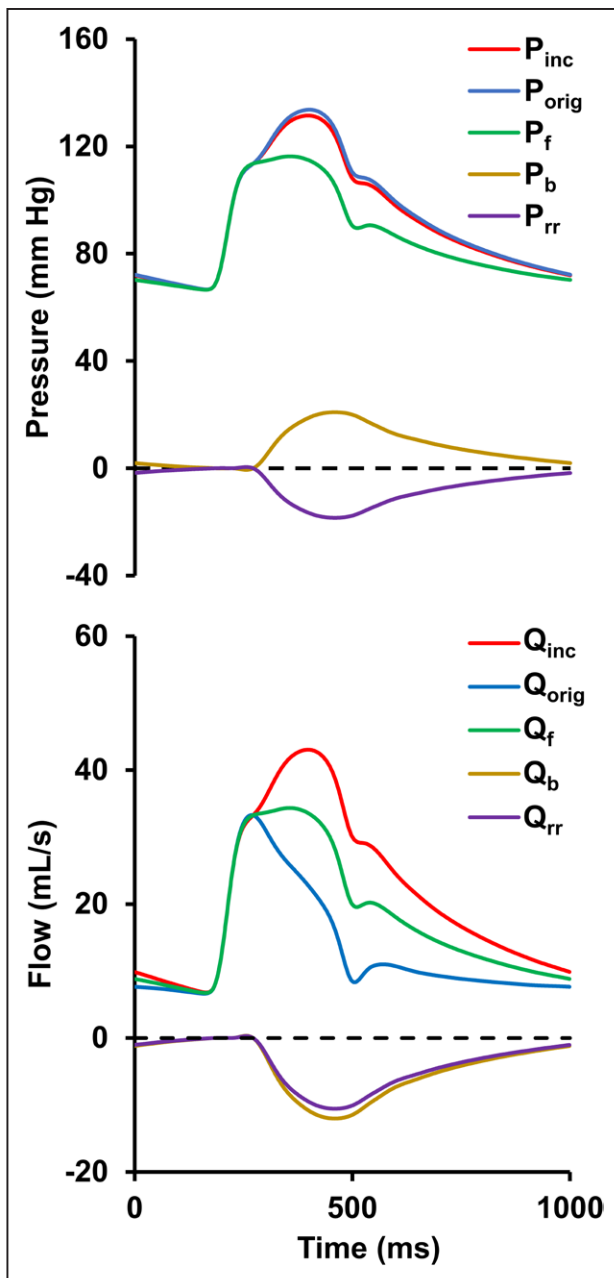
Figure 2. Waveform separation analysis in the proximal carotid.
Measured waveforms in the proximal carotid were separated into forward and backward pressure and flow waves. The forward waves were further separated into incident and rereflected components. The reflected and rereflected waves have nearly equal amplitude and opposite polarity, resulting in a measured pressure wave that is nearly the same as the incident pressure wave. The reflected and rereflected flow waves are the same polarity and nearly equal amplitude, resulting in a measured flow wave that is substantially different from the incident flow. P_b indicates backward pressure; P_f, forward pressure; P_{inc}, incident pressure; P_{orig}, derived pressure at carotid origin; P_{rr}, rereflected pressure; Q_b, backward flow; Q_f, forward flow; Q_{inc}, incident flow; Q_{orig}, derived flow at carotid origin; and Q_{rr}, rereflected flow.

RESULTS

Clinical characteristics of the 668 participants in our cohort of older adults are presented in Table 1.

Hemodynamic variables are summarized in Table 2. Pulse pressure and aortic characteristic impedance were relatively high in this sample. Carotid peripheral resistance was 5-fold higher than aortic, consistent with the observation that ≈20% of cardiac output goes to the brain. However, carotid characteristic impedance was an order of magnitude greater than aortic, resulting in a 2-fold higher normalized impedance in the carotid (Table 2). Mean power, pulsatile power, and pulsatile power as a percentage of total were markedly lower in the carotid than the proximal aorta (Table 2).

Figure 2 illustrates size and shape of forward, backward, rereflected, incident, and measured waves at the carotid origin. A small difference in size and shape of incident and measured pressure waveforms contrasted with major differences in size and shape of incident and measured flow. When cases were stratified by sex-specific median carotid flow transmission coefficient $(1-\Gamma_2)$ (0.12 in men and 0.10 in women), incident pulsatile power at the carotid origin was higher in individuals with high versus low carotid flow transmission coefficient $(1-\Gamma_2)$ (41.7±18.9 versus 30.0±14.5 mW, P<0.001). Table S1 summarizes the contribution of components of power to the transformation from incident to net power dissipated in the carotid circulation in the full sample. The in-phase components of incident and rereflected pressure and flow contributed to forward power transmission. However, the cross terms, $Pinc_{Car} \times Qrr_{Car}$ and $Prr_{Car} \times Qinc_{Car}$, combined to reduce forward power transmission within the carotid (Table S1), resulting in a net reduction of transmitted power as a result of rereflection (−12.5±8.1 mW). Forward power ($P_f \times Q_f$) was further reduced by local wave reflection ($P_b \times Q_b$), resulting in the net power dissipation (Table S1). The cross terms of forward and reflected waves were equal in amplitude but opposite in sign and, therefore, had no effect on net transmitted power. The proportion of incident power ultimately transmitted into and dissipated in the carotid circulation (54±13%) was closely related to the distal carotid reflection factor (R=−0.898, P<0.001).

Results of multivariable linear regression models for carotid flow SD and pulsatile power are presented in Table 3. Candidate exposures included central pulse pressure, carotid flow transmission coefficient $(1-\Gamma_2)$, carotid distal reflection factor, and heart rate. Carotid pulse pressure, carotid flow transmission coefficient $(1-\Gamma_2)$, and heart rate were positively related, and carotid distal reflection factor was negatively related to both carotid flow SD and pulsatile power (Table 3). In a separate model that adjusted for age and distal carotid resistance, higher carotid characteristic impedance was associated with lower carotid distal reflection factor (R=−0.366, P<0.001), suggesting that increased carotid stiffness reduced the impedance gradient and distal wave reflection within the carotid system.

Table 1. Characteristics of the Sample

Variable	Value
Sample size	668
Women, N (%)	378 (57)
Age, y	75±4
Height, cm	168±9
Weight, kg	76±14
Waist, cm	100±11
Body mass index, kg/m²	27±4
Cholesterol, mmol/L	5.4±1.1
HDL, mmol/L	1.6±0.4
Triglycerides, mmol/L	1.1±0.6
Glucose, mmol/L	5.7±1.2
Medical history, n (%)	
Coronary heart disease	113 (17)
Diabetes	67 (10)
Treated hypertension	396 (59)
Statin use	159 (24)
Current smoker	76 (11)
Education level, n (%)	
Elementary	141 (21)
Secondary	354 (53)
Junior college	98 (15)
University	75 (11)
GDS score, median (25%–75%)	2 (1–3)
MMSE, median (25%–75%)	27 (26–29)

GDS indicates geriatric depression scale; HDL, high-density lipoprotein; and MMSE, minimental state examination score.

As previously reported,[8] brain magnetic resonance imaging revealed the following segmental volumes as a percentage of intracranial volume: total parenchyma, 73±4%; gray matter, 46±3%; and white matter, 26±2%. Median white matter hyperintensity volume was 11 (25th–75th percentiles: 6–22) mL, or −4.9±0.9 as a natural logarithm transformed percentage of intracranial volume. Relations of carotid flow SD and carotid pulsatile power percentage with measures of brain structure and function are presented in Table 4. Higher carotid flow SD was associated with lower total parenchyma and white matter volumes, while higher pulsatile power percentage was associated with lower white matter volumes. Neither variable was related to gray matter or white matter hyperintensity volume (Table 4). Both measures were associated with lower scores on memory and executive function tests, while only flow SD was related to lower scores on tests of processing speed (Table 4). In the subset of participants with the foregoing brain measures and cardiac echocardiography (N=334), in a model that adjusted for the same covariates, higher carotid flow transmission coefficient $(1-\Gamma_2)$ and higher carotid power transmission coefficient $(1+\Gamma_1)(1-\Gamma_2)$ were associated with lower white matter volume (R=−0.156, P=0.005 and R=−0.140, P=0.012, respectively).

Table 2. Hemodynamic Variables

Variable	Value±SD
Blood pressure, mm Hg	
Systolic	139±19
Diastolic	66±10
Mean	94±12
Central pulse pressure	69±21
Heart rate, beats/min	62±10
Aortic pressure-flow measures*	
Mean flow, mL/s	63.4±15.1
Resistance, dyne×s/cm⁵	2106±553
Characteristic impedance, dyne×s/cm⁵	259±96
Normalized impedance, ratio	0.13±0.04
Pulsatility index, ratio	4.5±0.6
Flow SD, mL/s	98.7±21.8
Total power, mW	1062±301
Mean power, mW	798±220
Pulsatile power, mW	265±107
Pulsatile power percent, %	25±5
Distal reflection factor, ratio	0.34±0.10
Carotid pressure-flow measures	
Mean flow, mL/s	13.5±3.3
Resistance, dyne×s/cm⁵	9972±2903
Characteristic impedance, dyne×s/cm⁵	2504±879
Normalized impedance, ratio	0.26±0.07
Pulsatility index, ratio	1.8±0.5
Flow SD, mL/s	7.2±2.0
Total power, mW	189±51
Mean power, mW	170±46
Pulsatile power, mW	19±10
Pulsatile power percent, %	10±4
Distal reflection factor, ratio	0.41±0.11
Bifurcation reflection coefficient (Γ_1), unitless*	0.06±0.03
Carotid flow transmission coefficient $(1-\Gamma_2)$, unitless*	0.11±0.04
Carotid power transmission coefficient $(1+\Gamma_1)(1-\Gamma_2)$, unitless*	0.12±0.04

*In a subset of 210 men and 261 women with echocardiographic data.

DISCUSSION

We performed a detailed analysis of wave reflection and power transmission at the origin of a FGBA arising from the aorta, using a lumped model of the right and left common carotid circulation as an example. This general aortic structural element, consisting of a low characteristic impedance proximal aortic parent vessel that bifurcates asymmetrically into a high characteristic impedance FGBA and low characteristic impedance distal aortic segment, repeats along the full length of the aorta, with the exception of the terminal aorta, which bifurcates symmetrically into the 2 iliac arteries.[29] The sequential asymmetrical bifurcations are characterized

Table 3. Relations of Arterial Measures With Carotid Pulsatility

Variable	Carotid flow SD		Carotid pulsatile power	
	B±SE	P value	B±SE	P value
Carotid mean flow	0.483±0.032	<0.001	…	
Carotid mean power	…		0.326±0.021	<0.001
Central pulse pressure	0.459±0.037	<0.001	0.895±0.021	<0.001
Carotid flow transmission coefficient $(1-\Gamma_2)$	0.261±0.030	<0.001	0.122±0.017	<0.001
Heart rate	0.220±0.031	<0.001	0.099±0.018	<0.001
Carotid distal reflection factor	−0.062±0.029	0.036	−0.209±0.017	<0.001
Model R^2	0.686	<0.001	0.896	<0.001

Models also adjust for age, height, weight, high-density lipoprotein cholesterol level, blood glucose, hypertension treatment, use of statin drugs, mean arterial pressure, and current smoking. Mean flow and mean power were entered into the models for flow SD and pulsatile power, respectively, before stepwise entry of additional exposure variables. All continuous variables were converted to sex-standardized Z scores. Carotid flow SD, carotid pulsatile power, central pulse pressure, mean carotid flow, and mean carotid power were natural log transformed.

Table 4. Relations of Arterial Measures With Brain Structure and Function

Variable	Carotid flow SD		Carotid pulsatile power	
	R	P value	R	P value
Brain structure				
Total brain parenchyma	−0.094	0.017	−0.062	0.113
Gray matter	−0.047	0.230	−0.016	0.677
White matter	−0.130	<0.001	−0.093	0.018
White matter hyperintensity volume	0.068	0.081	0.010	0.794
Cognitive function				
Memory	−0.161	<0.001	−0.153	<0.001
Speed	−0.091	0.020	−0.053	0.174
Executive function	−0.153	<0.001	−0.134	<0.001

Adjusted for age, height, weight, high-density lipoprotein cholesterol level, blood glucose, hypertension treatment, use of statin drugs, heart rate, mean arterial pressure, current smoking, presence of depressive symptoms, and education. Carotid flow SD was adjusted for mean flow. Carotid pulsatile power was adjusted for mean power. Carotid flow SD and carotid pulsatile power were natural log transformed and converted to sex-specific Z scores. White matter hyperintensity volume was transformed by using the natural logarithm.

by a low bifurcation reflection coefficient (Γ_1), a very high FGBA reflection coefficient (Γ_2), and a low distal aortic reflection coefficient (Γ_3). The low bifurcation reflection coefficient (Γ_1) limits wave reflection within the proximal aortic segment and minimizes transmitted pressure amplification in the daughter branches. Since pressure at the origins of the daughter branches must be equivalent, the pressure level is effectively clamped and the low flow transmission coefficient of the FGBA $(1-\Gamma_2)$ has a dominant effect on flow, markedly limiting pulsatile flow transmission into this branch. The combination of minimal pressure amplification and marked attenuation of flow pulsatility results in a large net reduction in pulsatile power transmitted into the FGBA circulation. Furthermore, reflected waves arising in the distal vasculature of the FGBA circulation encounter a strong negative rereflection coefficient $(-\Gamma_2)$ at the FGBA origin. Resulting rereflected waves minimally amplify pressure and markedly attenuate flow, a secondary effect that further limits pulsatile power transmission into the FGBA vascular bed. Higher aortic stiffness increases the local carotid flow transmission coefficient $(1-\Gamma_2)$, resulting in higher carotid flow pulsatility and greater dissipation of pulsatile power in the carotid circulation. Greater carotid flow pulsatility and pulsatile power dissipation were associated with evidence of microvascular damage in the brain and reduced performance on cognitive testing. The foregoing observations are consistent with the hypothesis that aortic stiffening reduces the local impedance gradient at the origin of FGBAs and increases harmful pulsatile power transmission into the microcirculation, resulting in target organ damage and dysfunction.

The low flow transmission coefficient at the origin of the FGBA $(1-\Gamma_2)$ represents the first barrier to entry of pulsatile power into the FGBA circulation. Some have argued that the concept that high levels of wave reflection, which could increase load on the heart, are required to protect distal vascular beds is at odds with optimal ventricular performance and design.[10] The present analysis demonstrates that arterial system design protects the downstream microcirculation while also limiting pulsatile load on the heart. Our low observed values of bifurcation reflection coefficient (Γ_1), ≈6%, are consistent with the previously described phenomenon of impedance matching for bifurcations in the forward direction,[12–15] and imply minimal additional reflected wave loading of the heart. In addition, researchers have previously suggested that wave reflection at aortic bifurcations has a trivial effect on transmitted pulsatile power because bifurcation reflection coefficients (Γ_1) tend to be small.[9,10] Others have observed that transmitted pulsatile pressure would actually be increased by wave reflection at multiple successive junctions, exposing target organs to potentially harmful pressure pulsatility.[9–11] It is important to note, however, that while pulsatile pressure transmission increases in proportion to the bifurcation reflection coefficient (Γ_1), which is small, transmitted pulsatile flow and power decrease in proportion to the much larger FGBA reflection coefficient (Γ_2). As a result, flow wave amplitude in the carotid was reduced 9-fold relative to the aorta while pressure wave amplitude increased by only 6%, resulting in a marked net reduction in pulsatile power entering the carotid branch. Thus, while the majority of hydraulic power is transmitted through the bifurcation, the low FGBA flow transmission coefficient $(1-\Gamma_2)$

ensures this forward-traveling power is distributed unequally to the 2 daughter branches, with the FGBA receiving a disproportionately smaller amount of pulsatile power than the distal aorta, despite relatively high mean flow in the case of the carotid circulation, leading to a major reduction in relative pulsatility of flow and power in the FGBA.

Beyond the initial effect of asymmetrical pulsatile flow allocation, the large negative rereflection coefficient for retrograde waves at the FGBA origin ($-\Gamma_2$) further limits pulsatile power entering the FGBA circulation. Previous work has suggested that the majority of local reflected wave hydraulic power within FGBA vascular beds is rereflected downstream and therefore trapped in the FGBA circulation.[12,14,15] Forward pulsatile hydraulic power ($Pf_{Car} \times Qf_{Car}$) represents the sum of 4 incident and rereflected power terms (Table S1). However, forward power is substantially less than incident power ($Pinc_{Car} \times Qinc_{Car}$). Rereflected power ($Prr_{Car} \times Qrr_{Car}$) does contribute to forward-traveling power; however, its effect is outweighed by the large negative contribution of the 2 cross terms (Table S1). Thus, while rereflection traps a small component of power within the FGBA circulation, it prevents a substantially greater component of pulsatile power from entering the local circulation, resulting in a net beneficial effect in terms of reducing flow pulsatility and pulsatile power in the downstream microcirculation.

Reflection within the carotid bed and rereflection at the carotid origin contribute to the distinctive, marked divergence in shape between pressure and flow in the carotids. The large, negative rereflection coefficient for retrograde waves at the origin of a daughter artery ($-\Gamma_2$) causes the reflected wave to rereflect as a forward-traveling expansion wave that reduces forward pressure and forward flow. Therefore, reflected waves arising from the distal carotid bed amplify pressure, but are nearly canceled by simultaneous rereflection at the carotid origin, resulting in minimal difference between incident and measured pressure waves (Figure 2). Conversely, the attenuation of measured flow by reflected flow waves is nearly doubled by the rereflected flow waves (Figure 2).

Net flow pulsatility entering the carotid branch correlates with adverse measures of brain structure and cognitive function, with the notable exceptions of gray matter volume and white matter hyperintensity volume (Table 3). Cortical gray matter is perfused by perforating branches arising from the long, circuitous pial arteries, which would be expected to effectively damp pulsatile energy proximal to the microcirculation. In contrast, white matter is perfused by short perforators arising directly from the circle of Willis and proximal segments of the major intracranial arteries. These shorter pathways are much less able to damp pressure and flow pulsatility. White matter hyperintensity volume appears to have a more complicated relation with pulsatility, correlating with neither flow nor power pulsatility in the present study. However, a prior analysis of this cohort has related white matter hyperintensity volume to higher carotid-femoral pulse wave velocity.[8]

An increase in the stiffness of FGBAs, such as the carotid and renal arteries, should increase impedance mismatch between the aorta and the specific FGBA, as assessed by Γ_2, thereby protecting the downstream microcirculation. However, greater carotid stiffness has been associated with measures of downstream target organ damage.[30,31] Carotid arteries tend to stiffen in parallel with the aorta,[32] which could maintain a similar impedance mismatch and local carotid flow transmission coefficient ($1-\Gamma_2$) at the aorta-carotid bifurcation. However, aortic stiffening simultaneously increases pulse pressure and pulsatile power throughout the system. Furthermore, we have shown that carotid stiffening reduces distal wave reflection in the local vascular bed and hence limits the protective effects of reflection and rereflection within the carotid circulation. Conflicting favorable and deleterious effects of carotid stiffening may render isolated assessment of carotid stiffness a suboptimal approach for assessing cerebrovascular risk. In addition, isolated stiffening of the common carotid arteries likely would not provide a solution to the underlying problems of excessive pulsatility due to aortic stiffening and could be deleterious. Aortic stiffness, therefore, represents the best risk measure and target for interventions aimed at decreasing harmful pulsatile power transmission into the brain.

Limitations

There are limitations to this study that should be considered. We computed aortic characteristic impedance by using a measured common carotid artery pressure paired with the aortic flow, which will tend to overestimate aortic characteristic impedance by a factor comparable to the local bifurcation reflection coefficient in the proximal aorta (Γ_1). We aggregated flows from the right and left carotids and assumed that the right subclavian artery arose distal to the aggregated carotids, which means that our estimate for aortic characteristic impedance just proximal to the combined carotids was modestly underestimated. Since each of these errors was ≈4% to 6% in opposite directions, the net effect was likely very modest. In addition, we assumed that the right carotid arose directly from the aorta rather than the brachiocephalic. To validate this assumption, we compared the arrival times and cross-correlation of right and left carotid flow waveforms. The arrival times were nearly synchronous (78.8±15.2 versus 80.8±16.1 ms), and the cross-correlation of the 2 waveforms was quite high (R=0.97), consistent with our assumption that the origin of the right common carotid from the brachiocephalic trunk minimally affects carotid flow waveform morphology and timing.

ARTERIAL STIFFNESS

Segment delays within the ascending aorta and proximal carotid were not measured directly but rather were estimated from the overall foot-foot delay between aortic and carotid flows, assuming that waves propagating through the aorta reached the origin of the carotid at approximately the midpoint of this delay. However, these delays were relatively short and, therefore, changes in pressure and flow shape as a result of rephasing forward and reflected components to estimate pressure and flow at the carotid origin were relatively small. Echocardiography was performed in a random subset of half of our participants. As a result, we have limited statistical power to assess relations of reflection coefficients, such as Γ_2, with brain variables. To address this limitation, we related reflection coefficients to flow and power transmission in the subset with echocardiography; we then related measures of pulsatile flow and power to brain variables in the full sample.

The average age of participants in this study was 75 years and the sample exhibited many aortic and brain structural and functional changes commonly seen with aging. In addition, the sample included only white individuals of European descent. Therefore, our results may not be generalizable to younger people with markedly lower aortic stiffness or to other races or ethnicities. Studies in younger cohorts of varied racial and ethnic composition will be required.

Perspectives

The structure of the aorta-carotid interface, as an example of a highly asymmetrical bifurcation, is optimally designed for minimal augmentation of transmitted pulsatile pressure with marked attenuation of transmitted pulsatile flow and pulsatile power in the FGBA. Reflections arising from the distal carotid circulation and rereflection at the carotid origin further decrease power transmitted into the cerebrovasculature. Aortic stiffening leads to a decrease in the impedance gradient between the proximal aorta and the common carotid arteries, and, crucially, to an increase in the local flow transmission coefficient of the FGBA $(1-\Gamma_2)$, while the overall reflection coefficient of the bifurcation (Γ_1) remains small. Decreased local reflection allows for greater pulsatile power transmission into the FGBA. Pulsatile power and specifically the pulsatile flow component are associated with presence of microvascular brain lesions and reduced performance in various cognitive domains. We suggest that relations between aortic and FGBA pulsatile power follow from a general design feature of the aorta and FGBAs and applies to other vascular beds supplied by high impedance FGBAs arising from the much larger aorta.

ARTICLE INFORMATION

Affiliations

From the Cardiovascular Engineering, Inc, Norwood, MA (M.A.H., J.D.G., G.F.M.); Department of Radiology, Leiden University Medical Center, the Netherlands (M.A.v.B.); Icelandic Heart Association, Kopavogur, Iceland (S.S., V.G.); Faculty of Medicine, University of Iceland, Reykjavik (V.G.); and Intramural Research Program, Laboratory of Epidemiology and Population Sciences, National Institute on Aging, Baltimore, MD (L.J.L.).

Disclosures

G.F. Mitchell is the president of Cardiovascular Engineering Inc, a company that designs and manufactures devices that measure vascular stiffness, and reported serving as a consultant to and receiving honoraria and grant support from Novartis, Servier, Merck, Bayer, and the National Institutes of Health. M.J. Haidar and J.D. Gotal are employees of Cardiovascular Engineering Inc. The other authors report no conflicts.

REFERENCES

1. Alzheimer's Association. 2020 Alzheimer's disease facts and figures. *Alzheimer's Dement.* 2020;16:391–460.
2. Gorelick PB, Scuteri A, Black SE, Decarli C, Greenberg SM, Iadecola C, Launer LJ, Laurent S, Lopez OL, Nyenhuis D, et al; American Heart Association Stroke Council, Council on Epidemiology and Prevention, Council on Cardiovascular Nursing, Council on Cardiovascular Radiology and Intervention, and Council on Cardiovascular Surgery and Anesthesia. Vascular contributions to cognitive impairment and dementia: a statement for healthcare professionals from the American Heart Association/American Stroke Association. *Stroke.* 2011;42:2672–2713. doi: 10.1161/STR.0b013e3182299496
3. Climie RED, Picone DS, Blackwood S, Keel SE, Qasem A, Rattigan S, Sharman JE. Pulsatile interaction between the macro-vasculature and micro-vasculature: proof-of-concept among patients with type 2 diabetes. *Eur J Appl Physiol.* 2018;118:2455–2463. doi: 10.1007/s00421-018-3972-2
4. Mitchell GF. Effects of central arterial aging on the structure and function of the peripheral vasculature: implications for end-organ damage. *J Appl Physiol (1985).* 2008;105:1652–1660. doi: 10.1152/japplphysiol.90549.2008
5. Mitchell GF. Aortic stiffness, pressure and flow pulsatility, and target organ damage. *J Appl Physiol (1985).* 2018;125:1871–1880. doi: 10.1152/japplphysiol.00108.2018
6. Woodard T, Sigurdsson S, Gotal JD, Torjesen AA, Inker LA, Aspelund T, Eiriksdottir G, Gudnason V, Harris TB, Launer LJ, et al. Mediation analysis of aortic stiffness and renal microvascular function. *J Am Soc Nephrol.* 2015;26:1181–1187. doi: 10.1681/ASN.2014050450
7. Londono-Hoyos F, Zamani P, Beraun M, Vasim I, Segers P, Chirinos JA. Effect of organic and inorganic nitrates on cerebrovascular pulsatile power transmission in patients with heart failure and preserved ejection fraction. *Physiol Meas.* 2018;39:044001. doi: 10.1088/1361-6579/aab2ef
8. Mitchell GF, van Buchem MA, Sigurdsson S, Gotal JD, Jonsdottir MK, Kjartansson Ó, Garcia M, Aspelund T, Harris TB, Gudnason V, et al. Arterial stiffness, pressure and flow pulsatility and brain structure and function: the Age, Gene/Environment Susceptibility–Reykjavik study. *Brain.* 2011;134(pt 11):3398–3407. doi: 10.1093/brain/awr253
9. Chirinos JA. Deep phenotyping of systemic arterial hemodynamics in HFpEF (Part 2): clinical and therapeutic considerations. *J Cardiovasc Transl Res.* 2017;10:261–274. doi: 10.1007/s12265-017-9736-2
10. Phan TS, Li JK, Segers P, Reddy-Koppula M, Akers SR, Kuna ST, Gislason T, Pack AI, Chirinos JA. Aging is associated with an earlier arrival of reflected waves without a distal shift in reflection sites. *J Am Heart Assoc.* 2016;5:e003733.
11. Kondiboyina A, Smolich JJ, Cheung MMH, Westerhof BE, Mynard JP. Conduit arterial wave reflection promotes pressure transmission but impedes hydraulic energy transmission to the microvasculature. *Am J Physiol Heart Circ Physiol.* 2020;319:H66–H75. doi: 10.1152/ajpheart.00733.2019
12. Alastruey J, Parker KH, Peiro J, Sherwin SJ. Analysing the pattern of pulse waves in arterial networks: a time-domain study. *J Eng Math.* 2009;64:331–351.

13. Baksi AJ, Davies JE, Hadjiloizou N, Baruah R, Unsworth B, Foale RA, Korolkova O, Siggers JH, Francis DP, Mayet J, et al. Attenuation of reflected waves in man during retrograde propagation from femoral artery to proximal aorta. *Int J Cardiol*. 2016;202:441–445. doi: 10.1016/j.ijcard.2015.09.064

14. Davies JE, Alastruey J, Francis DP, Hadjiloizou N, Whinnett ZI, Manisty CH, Aguado-Sierra J, Willson K, Foale RA, Malik IS, et al. Attenuation of wave reflection by wave entrapment creates a "horizon effect" in the human aorta. *Hypertension*. 2012;60:778–785. doi: 10.1161/HYPERTENSIONAHA.111.180604

15. Sherwin SJ, Franke V, Peiro J, Parker K. One-dimensional modelling of a vascular network in space-time variables. *J Eng Math*. 2003;47:217–250.

16. Harris TB, Launer LJ, Eiriksdottir G, Kjartansson O, Jonsson PV, Sigurdsson G, Thorgeirsson G, Aspelund T, Garcia ME, Cotch MF, et al. Age, Gene/Environment Susceptibility-Reykjavik Study: multidisciplinary applied phenomics. *Am J Epidemiol*. 2007;165:1076–1087. doi: 10.1093/aje/kwk115

17. de Groot JC, de Leeuw FE, Oudkerk M, van Gijn J, Hofman A, Jolles J, Breteler MM. Cerebral white matter lesions and cognitive function: the Rotterdam Scan Study. *Ann Neurol*. 2000;47:145–151. doi: 10.1002/1531-8249(200002)47:2<145::aid-ana3>3.3.co;2-g

18. Saczynski JS, Jonsdottir MK, Sigurdsson S, Eiriksdottir G, Jonsson PV, Garcia ME, Kjartansson O, van Buchem MA, Gudnason V, Launer LJ. White matter lesions and cognitive performance: the role of cognitively complex leisure activity. *J Gerontol A Biol Sci Med Sci*. 2008;63:848–854. doi: 10.1093/gerona/63.8.848

19. Schaie KW, Maitland SB, Willis SL, Intrieri RC. Longitudinal invariance of adult psychometric ability factor structures across 7 years. *Psychol Aging*. 1998;13:8–20. doi: 10.1037/0882-7974.13.1.8

20. Scher AI, Gudmundsson LS, Sigurdsson S, Ghambaryan A, Aspelund T, Eiriksdottir G, van Buchem MA, Gudnason V, Launer LJ. Migraine headache in middle age and late-life brain infarcts. *JAMA*. 2009;301:2563–2570. doi: 10.1001/jama.2009.932

21. Sigurdsson S, Aspelund T, Forsberg L, Fredriksson J, Kjartansson O, Oskarsdottir B, Jonsson PV, Eiriksdottir G, Harris TB, Zijdenbos A, et al. Brain tissue volumes in the general population of the elderly: the AGES-Reykjavik study. *Neuroimage*. 2012;59:3862–3870. doi: 10.1016/j.neuroimage.2011.11.024

22. Wilson RS, Bennett DA, Beckett LA, Morris MC, Gilley DW, Bienias JL, Scherr PA, Evans DA. Cognitive activity in older persons from a geographically defined population. *J Gerontol B Psychol Sci Soc Sci*. 1999;54:P155–P160. doi: 10.1093/geronb/54b.3.p155

23. Kelly R, Fitchett D. Noninvasive determination of aortic input impedance and external left ventricular power output: a validation and repeatability study of a new technique. *J Am Coll Cardiol*. 1992;20:952–963. doi: 10.1016/0735-1097(92)90198-v

24. Mitchell GF, Parise H, Vita JA, Larson MG, Warner E, Keaney JF Jr, Keyes MJ, Levy D, Vasan RS, Benjamin EJ. Local shear stress and brachial artery flow-mediated dilation: the Framingham Heart Study. *Hypertension*. 2004;44:134–139. doi: 10.1161/01.HYP.0000137305.77635.68

25. Dujardin JP, Stone DN. Characteristic impedance of the proximal aorta determined in the time and frequency domain: a comparison. *Med Biol Eng Comput*. 1981;19:565–568. doi: 10.1007/BF02442770

26. Nakayama Y, Nakanishi N, Sugimachi M, Takaki H, Kyotani S, Satoh T, Okano Y, Kunieda T, Sunagawa K. Characteristics of pulmonary artery pressure waveform for differential diagnosis of chronic pulmonary thromboembolism and primary pulmonary hypertension. *J Am Coll Cardiol*. 1997;29:1311–1316. doi: 10.1016/s0735-1097(97)00054-5

27. Mynard JP, Smolich JJ. Novel wave power analysis linking pressure-flow waves, wave potential, and the forward and backward components of hydraulic power. *Am J Physiol Heart Circ Physiol*. 2016;310:H1026–H1038. doi: 10.1152/ajpheart.00954.2015

28. Westerhof N, Sipkema P, van den Bos GC, Elzinga G. Forward and backward waves in the arterial system. *Cardiovasc Res*. 1972;6:648–656. doi: 10.1093/cvr/6.6.648

29. Alastruey J. Numerical assessment of time-domain methods for the estimation of local arterial pulse wave speed. *J Biomech*. 2011;44:885–891. doi: 10.1016/j.jbiomech.2010.12.002

30. Brisset M, Boutouyrie P, Pico F, Zhu Y, Zureik M, Schilling S, Dufouil C, Mazoyer B, Laurent S, Tzourio C, et al. Large-vessel correlates of cerebral small-vessel disease. *Neurology*. 2013;80:662–669. doi: 10.1212/WNL.0b013e318281ccc2

31. Romero JR, Beiser A, Seshadri S, Benjamin EJ, Polak JF, Vasan RS, Au R, DeCarli C, Wolf PA. Carotid artery atherosclerosis, MRI indices of brain ischemia, aging, and cognitive impairment: the Framingham study. *Stroke*. 2009;40:1590–1596. doi: 10.1161/STROKEAHA.108.535245

32. Paini A, Boutouyrie P, Calvet D, Tropeano AI, Laloux B, Laurent S. Carotid and aortic stiffness: determinants of discrepancies. *Hypertension*. 2006;47:371–376. doi: 10.1161/01.HYP.0000202052.25238.68